FRACKING THE CODE ON FLOWBACK FLUID

Undergraduate Research Thesis
Submitted in partial fulfillment of the requirements for graduation
with research distinction in Earth Sciences
in the undergraduate colleges of

The Ohio State University

By

Chandler J. Adamaitis
The Ohio State University
2017

Approved by

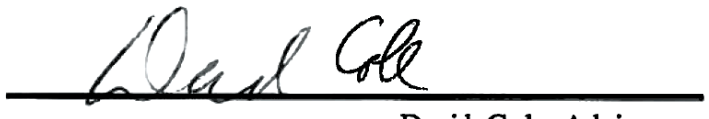

David Cole, Advisor

Sue Welch, Advisor

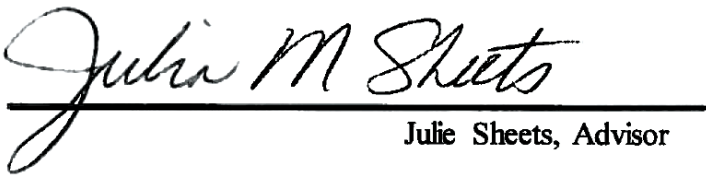

Julie Sheets, Advisor

TABLE OF CONTENTS

ABSTRACT

Hydraulic fracturing of shale generates brines with complex chemistries. As such, these fluids have trace metal constituents that can be rendered valuable if concentrated. This project used samples of hydraulic fracturing flowback fluid from the Utica/Point Pleasant formations in Ohio to analyze how different additives of acids and bases could influence precipitation and sequester trace metals. Flowback fluids were treated with sulfuric acid (H_2SO_4), phosphoric acid (H_3PO_4), hydrochloric acid (HCl), and sodium carbonate (Na_2CO_3), each in a high and low concentration. The fluids were allowed to react over several weeks and then the precipitates and the solutions were analyzed using scanning electron microscopy (SEM) and x-ray diffraction (XRD), and inductively coupled plasma optical emission spectrometry (ICP-OES) and inductively coupled plasma mass spectrometry (ICP-MS), respectively. Reacting hydraulic fracturing fluid with these acids and bases in different concentrations allowed for the precipitation of different minerals with variable elemental compositions. For example, low concentrations of H_2SO_4 resulted mainly in barite ($BaSO_4$) precipitation, while high H_2SO_4 resulted in precipitates of celestite ($SrSO_4$) and gypsum ($CaSO_4 \cdot 2H_2O$). Additionally, akaganeite ($Fe^{3+}O(OH,Cl)$) was found in the precipitates of the control sample and the high H_3PO_4 sample. This suggests that further research should focus on akaganeite as another phase that could sequester trace elements, because its crystal structure has large spaces that could accommodate such trace metals.

ACKNOWLEDGEMENTS

I would like to give a huge thank you to Sue Welch and Julie Sheets for their amazing advising and patience with me throughout this process. Also, thank you to David Cole and Anthony Lutton for help with experiments, analyses, and advising. XRD scans and SEM images were acquired at the Subsurface Energy Materials Characterization and Analysis Laboratory (SEMCAL); ICP-OES and ICP-MS analyses of hydraulic fracturing fluids were conducted at the Trace Element Research Laboratory (TERL), School of Earth Sciences, The Ohio State University. This project was made possible through funding from the Ohio Water Resource Center of the Office of Energy and Environment. A special thank you to Anne Carey and Derek Sawyer for all their help throughout the SURE program, and to Shell Exploration and Production Company for making the SURE program possible. Also, a personal thank you to my family and my friends Nikki Kinash and Seth Bryson for pushing me through the most stressful moments this semester; I could not have done it without you guys.

List of Figures

List of Tables

INTRODUCTION

Hydraulic fracturing of lateral wells in the Utica/Point Pleasant Shales to extract unconventional hydrocarbon resources is generating enormous quantities of natural gas, with approximately 744 billion cubic feet produced from 2011 through the 1st quarter of 2015 in Ohio alone (Riley, 2015). Also in Ohio, from 2008 to 2014, there have been 838 hydraulic fracturing wells drilled, resulting in the cumulative water use of 21.30Mm^3 (Chen & Carter, 2016). Across the United States, in those same years, there were approximately 80,047 hydraulic fracturing wells drilled that used 929.98Mm^3 of water (Chen & Carter, 2016). Although hydraulic fracturing operations often reuse the recovered flowback fluids, the eventual disposal of such fluids remains a problem due to their complex chemistry and potential toxicity. Deep injection of waste fluids is prevalent in Ohio and minimizing this activity and finding other mechanisms of disposal is of interest to the general public.

As gas is produced in the hydraulic fracturing process, the water recovered from wells is in the form of saline brines, typically with total dissolved solids (TDS) in the range 10s to 100s g/L (Nelson et al., 2015). These brines also contain elevated levels of trace elements such as barium, strontium, radium, transition metals and rare earth elements (REE) (Nelson et al., 2015). The goal of this study is to understand the evolution of the major and trace element compositions in flowback fluids as they age, either while sitting on a lab bench or in an onsite holding tank, and to determine the nature of mineral precipitation when chemicals are added. This would thereby potentially remove elements from the fluids via sorption and co-precipitation reactions.

With such high volumes of fluid being pumped in and out of these wells, it would be beneficial to remove anything that could be considered toxic or even economically valuable. For example, precipitating barite ($BaSO_4$) and celestite ($SrSO_4$) can be beneficial for treating flowback fluids because the barium and strontium in those minerals can be easily substituted with radium, a radioactive element of concern found in flowback fluids (Kondash et al., 2014). It would also be advantageous to determine the optimal conditions in which precipitates could sequester and concentrate valuable metals, including REE. Even though these metals occur in small quantities, the vast volumes of returned hydraulic fracturing flowback fluid (HFFF) could help concentrate these quantities to render them substantial enough to be economically valuable. Therefore, flowback brine from the hydraulic fracturing site was amended with different concentrations of acids and bases in order to induce mineral precipitation and then analyze the viability of these treatments.

GEOLOGIC SETTING

The Utica Shale is an organic-rich shale of Middle Ordovician age that is yielding large amounts of natural gas, natural gas liquids and crude oil to wells drilled in eastern Ohio and western Pennsylvania (King, n.d.).

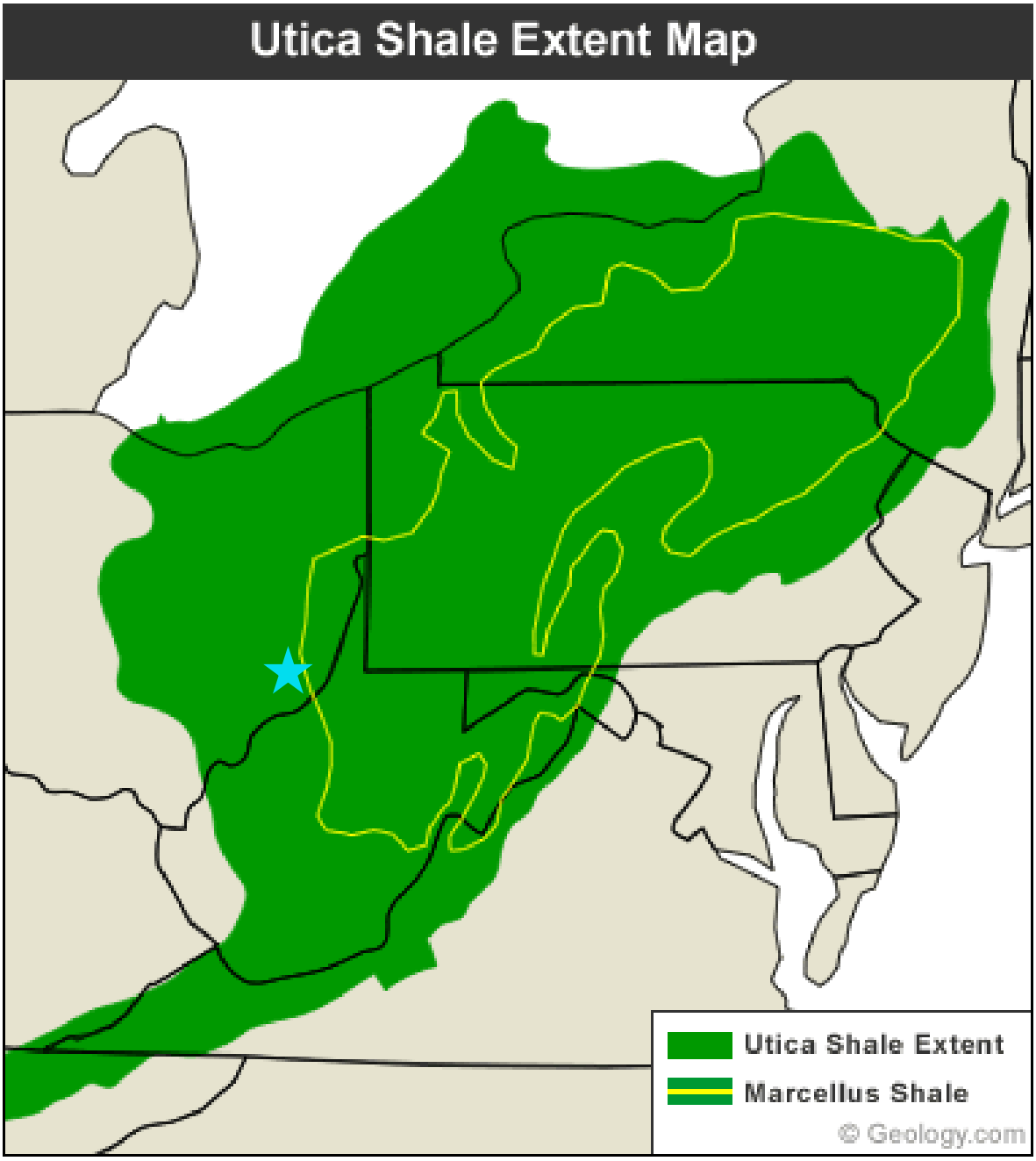

Figure 1: The green area on this map marks the geographic extent of the Utica Shale. Included in this extent are two the laterally equivalent units of the Point Pleasant Formation of Ohio and western Pennsylvania. The thin yellow line outlines the geographic extent of the Marcellus Shale Gas Play (King, n.d.). The blue star denotes the general location of the well from which the hydraulic fracturing flowback fluid used in this thesis was collected.

METHODS

Samples

Bulk flowback water samples were collected into five-gallon carboys with the assistance of Gulfport personnel (near the wellheads but after the phase separators) on September 8, 2016. Subsamples were taken for chemical analysis and the remainder was stored in the lab for several months prior to this study.

The large container of raw flowback fluid used for these experiments was vigorously shaken, as it had been sitting idle for a few months after collection and much of the suspended solids had settled to the bottom. Shaking ensured that the precipitate was re-suspended into the fluid to create a homogeneous mixture for sampling.

A 100mL graduated cylinder was used to measure nine 200mL aliquots of the flowback fluid which were placed in nine separate 250mL bottles. A 1mL trace metal spike (1ppm) was placed in each bottle. Each bottle was then given an additional additive as follows:

1. Control
2. Low [H_2SO_4] – 0.8mL at 2.5M
3. High [H_2SO_4] – 8.0 ml at 2.5M
4. Low [H_3PO_4] – 1.3mL at 1.5M
5. High [H_3PO_4] – 13mL at 1.5M
6. Low [HCl] – 2.0 mL at 1.0M
7. High [HCl] – 20mL at 1.0M
8. Low [Na_2CO_3] – 2mL at 1.0 M
9. High [Na_2CO_3] – 20 mL at 1.0 M

Water Analysis

Measurements of pH were taken for each bottle at the end of the experiment using an Orion pH meter. Liquid from each bottle was decanted to smaller beakers for pH measurement.

Aliquots of solution from each bottle were taken using a 10mL plastic syringe, avoiding the bottom precipitate, and filtered through a Whatman 25mm syringe filter with pore spaces of 0.45µm into clean 15mL Falcon polypropylene test tubes. Each tube was labeled with its sample number and the time at which the procedure was done for the first time: June 30, 2017 at approximately 3:30pm, representing T1.

This process was repeated, with extra care taken to avoid precipitate that was forming at the bottom of the bottles. At a sampling time, each tube was labeled with its corresponding number, date, and time: July 5, 2017 at approximately 11:30am, representing T2. A third round of samples were taken on July 12, 2017 at approximately 10:00am, representing T3.

Because the total dissolved solids (TDS) of these brines is about 200g/L, samples had to be diluted before analysis using a Perkin-Elmer Optima 3000DV and 4300DV Inductively Coupled Plasma Optical Emission Spectrometer (ICP-OES) and a Perkin-Elmer Sciex ELAN 6000 Inductively Coupled Plasma Mass Spectrometer (ICP-MS). Two dilutions were made for each sample. The first was a 201-fold dilution, done by using a pipette to place 100µL of each tube sample into a clean 50mL Falcon tube. Then, 20mL of 2% HNO_3 with a 10ppb spike of indium was placed in each tube so that the samples had enough trace elements to be detected by ICP-

MS. This set of diluted samples was made for analysis using ICP-MS and ICP-OES. The second set was a 2211-fold dilution made by taking 1mL of the 201-fold diluted solutions, adding it to a clean 50mL Falcon tube, and adding an additional 10mL of HNO_3, but without the indium spike. This set was analyzed using only ICP-OES.

Precipitate Analysis

In order to sample the precipitates, a clean pipette was placed in the bottom of the bottles to remove as much of the material as possible. This precipitate was then put into a clean plastic weighing dish and allowed to settle once more to allow the precipitate to separate from any solution that was accidentally introduced during pipetting. The precipitate was again selectively removed with the pipette and placed onto a 0.2μm polycarbonate filter on a filter flask. Once the liquid was filtered out, the remaining precipitate on the filter was rinsed two to three times with a few milliliters of distilled water to remove any remaining salt from the solution but to minimize the dissolution of the precipitates. This process was done twice for each solution in order to have one sample to analyze with scanning electron microscopy (SEM) using a FEI Quanta FEG 250 Field Emission Scanning Electron Microscope and one for X-ray diffraction (XRD) analysis with a PANalytical X'Pert Pro powder diffractometer. The SEM samples were transferred to small aluminum specimen mounts by putting double sided carbon tape on the mounts and then pressing the sticky carbon tape onto the dried, powdery samples on the filter. For XRD, the filters with precipitate on them were placed on cut glass slides with double-sided tape and then placed on modeling dough in order to fit them properly onto XRD sample mounts. All samples were then analyzed using SEM and XRD.

RESULTS

Flowback brine from the hydraulic fracturing site was amended with several different solutions in order to induce mineral precipitation. Analysis of the solution composition from these experiments showed that the concentrations of some elements did not change substantially over time after the various treatments, whereas others showed either a decrease or increase in concentration as a result of mineral precipitation/dissolution reactions. Analysis of the precipitates collected from the bench scale experiments at the end of the experiments by both XRD and SEM show changes in mineralogy that were consistent with the measured changes in solution composition determined using ICP-OES and ICP-MS analyses.

Water Chemistry

pH

In measuring pH, it was found that most of the samples where acid was added resulted in very low pH values ranging from 0.14 to 1.52 (**Table 1**). As expected, the samples with the higher added concentration of acid resulted in lower pH when compared to their low concentration counterpart. Even the control sample had a low pH value of 2.38, despite having no acid added to it. This fluid started out close to neutral as measured shortly after collection in the field, and therefore, must have acidified as it sat in the bottle through the oxidation and precipitation of iron. The low and high concentrations of Na_2CO_3 resulted in pH values of 6.26 and 6.64, respectively due to the buffering of the acidic flowback fluid with this base additive.

Sample	pH
Control	2.38
Low [H_2SO_4]	1.03
High [H_2SO_4]	0.14
Low [H_3PO_4]	1.32
High [H_3PO_4]	0.71
Low [HCl]	1.52
High [HCl]	0.42
Low [Na_2CO_3]	6.26
High [Na_2CO_3]	6.64

Table 1: pH measurements of each sample

Major Ions

ICP-OES analysis was used to measure major ion concentrations. Some of the changes observed over time for a single sample, and also between different samples could largely be attributed to dilution errors. For example, the sodium concentrations over time showed that there is slight variability, but, when compared to the precipitates, no evidence of sodium sequestration nor dissolution was found (**Figure 2**).

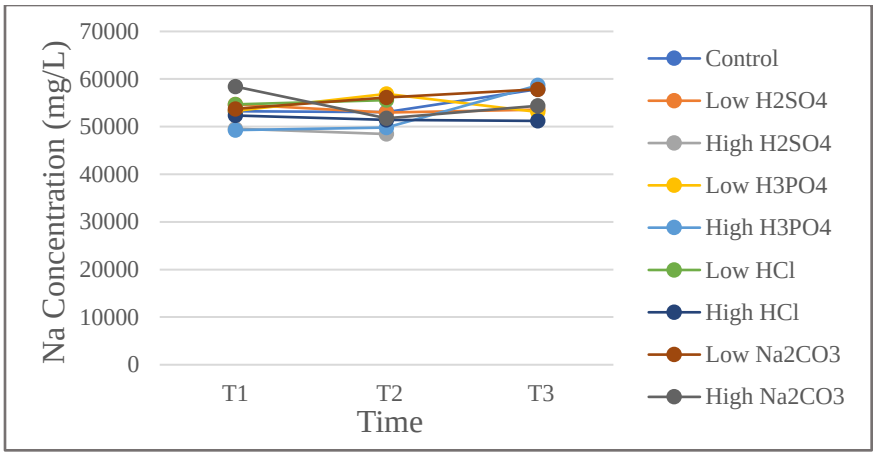

Figure 2: Comparison of sodium concentrations over time between the different samples.

The calcium concentration measurements also show some variability over time (**Figure 3**). For example, it appears that the calcium concentration went up and then back down in the low H_3PO_4 treatment. When compared to **Figure 2**, it appears this also happens with the sodium concentration; therefore, this can largely be attributed to a slight dilution error between each time samples. In other samples, however, it can be shown that the observed decreases in calcium over time are not due to the dilution effect. For example, for the high H_2SO_4 treatment, there is a decrease in the calcium concentration which is likely the result of precipitation of gypsum ($CaSO_4 \cdot 2H_2O$). Additionally, the high Na_2CO_3 treatment has a lowered calcium concentration through time due to the precipitation of calcite ($CaCO_3$).

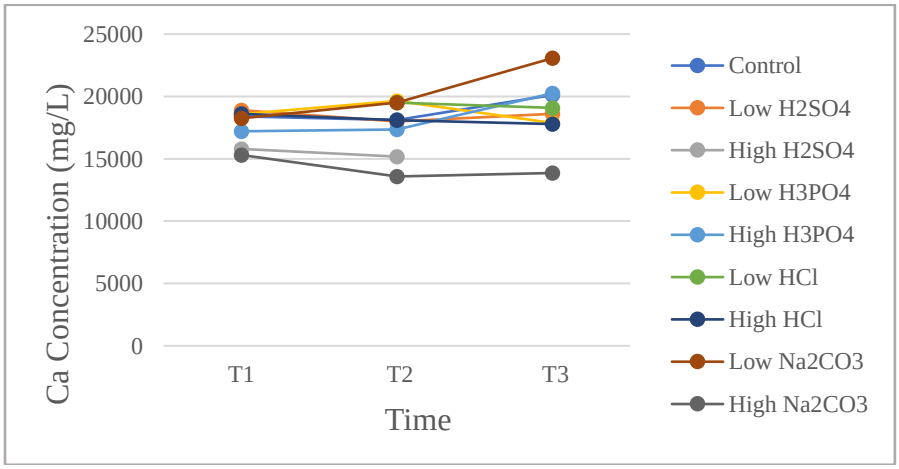

Figure 3: Comparison of calcium concentrations over time between the different samples.

Strontium concentration in most samples are relatively consistent over time (**Figure 4**), with the exception of the high H_2SO_4 sample. For this experiment, it appears that the strontium in the solution decreased shortly after the acid addition and then stayed fairly constant over time. This difference could be a result of the precipitation of celestite ($SrSO_4$). Additionally, the strontium concentration for the high Na_2CO_3 treatment is notably lower than the others, likely due to the co-precipitation with $CaCO_3$.

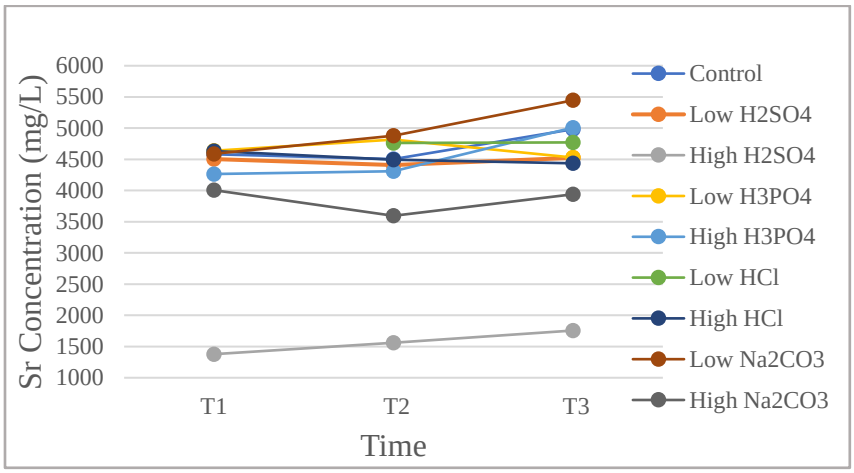

Figure 4: Comparison of strontium concentrations over time between the different samples.

Barium concentrations in most samples are constant over time except for the low H_2SO_4 and high H_2SO_4 treatments (**Figure 5**). Results from these two experiments suggest that the barium precipitated out of solution early in the experiments and then remained constant over time for the high treatment, but continued to decrease over time with the low addition. This difference suggests the precipitation of barite ($BaSO_4$). There is a slight drop in barium concentrations in the high Na_2CO_3 treatment, likely due to barium co-precipitation with $CaCO_3$.

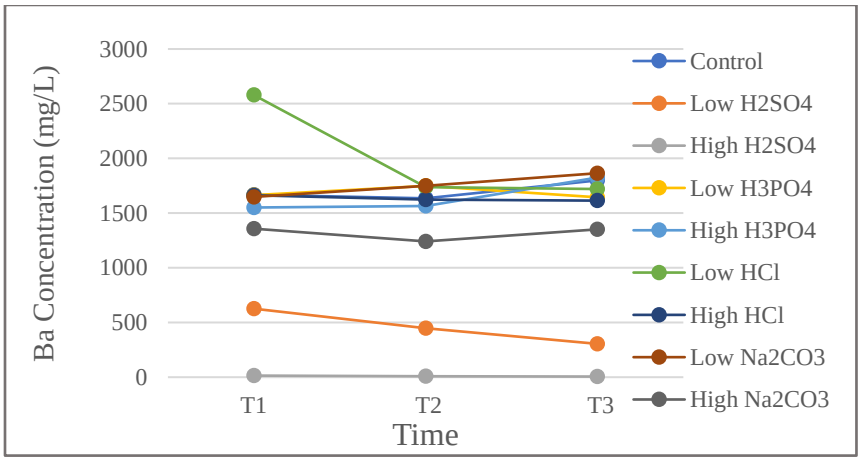

Figure 5: Comparison of barium concentrations over time between the different samples.

In contrast to other elements, the predominant behavior exhibited in the sample is an increase in iron over time, as seen in **Figure 6**. This change can largely be attributed to the high acidity of these samples, as depicted in **Table 1**, which would cause the iron to dissolve over time. In contrast to the other major elements measured, the concentration of Fe showed a systematic increase over time in all of the experiments where acid was added, except for the low H_3PO_4 treatment, because the acid conditions promoted the dissolution of the FeOOH phases that had formed from oxidation while the flowback fluid sat in the large carboy containers.

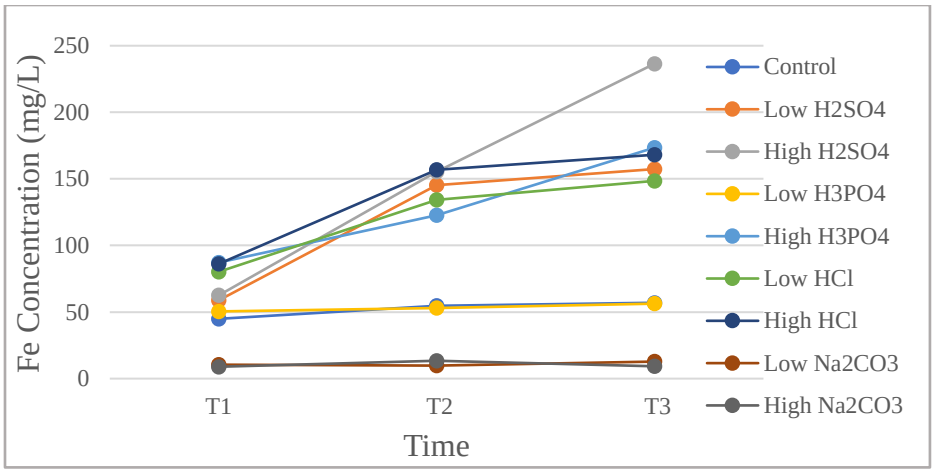

Figure 6: Comparison of iron concentrations over time between the different samples.

Minor Ions

Measurements of minor ions were made using ICP-MS. This analysis of trace metal concentrations of elements such as lithium show little change over time, indicating they were not sequestered into the precipitates as a result of the chemical additions (**Figure 7**). Similar results were found in measurements for elements such as rubidium, copper, nickel, and cesium (graphs attached in appendix). It would be expected that these elements would co-precipitate with iron oxyhydroxides, but instead they behave rather conservatively.

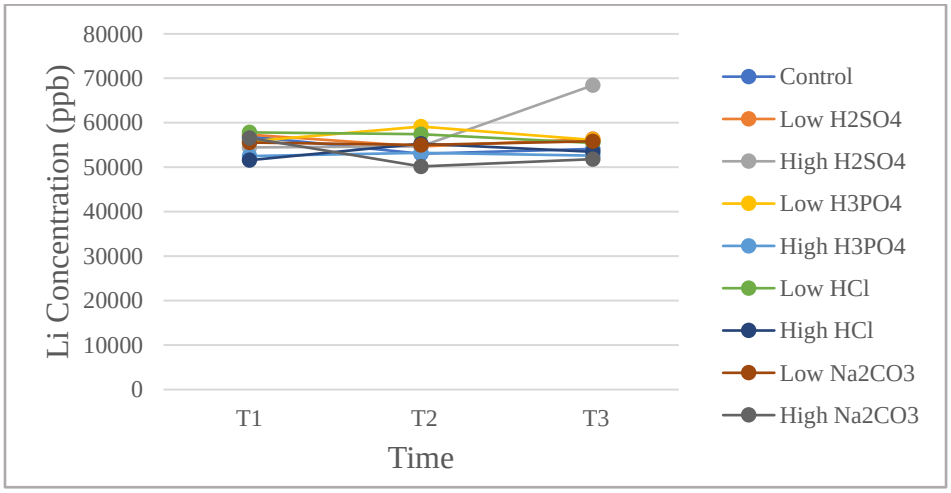

Figure 7: Comparison of lithium concentrations over time between the different samples.

Analysis of trace metal concentrations such as lanthanum differ from the previously discussed elements in that they do show slight changes over time, primarily in the low and high treatments of H_2SO_4 and Na_2CO_3 (**Figure 8**). The lanthanum continues to behave conservatively with respective to the HCl and H_3PO_4. Similar results were found in the measurements of gadolinium, samarium, and cerium (graphs attached in the appendix). These results can be linked to the

sorption and co-precipitation of these elements onto the minerals that precipitated in the respective treatments.

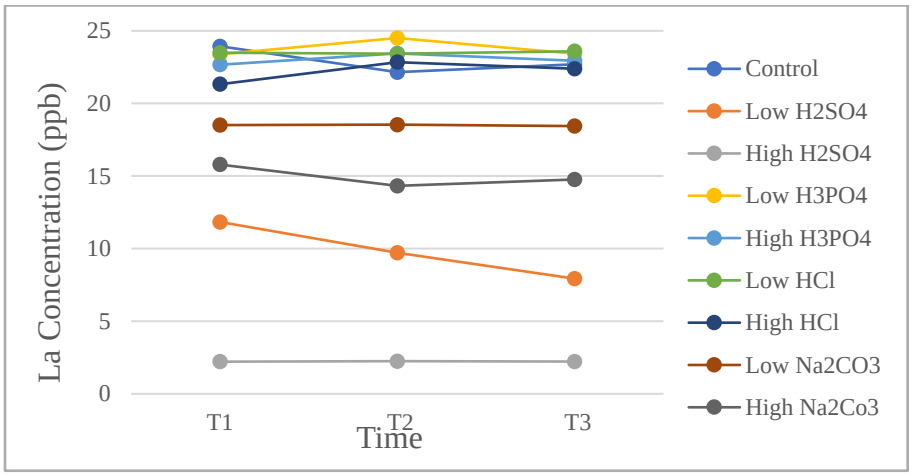

Figure 8: Comparison of lanthanum concentrations over time between the different samples.

Analysis of heavier elements, such as lutetium, indicate conservative concentrations through time for all treatments except the low and high additives of Na_2CO_3 (**Figure 9**). This suggests that lutetium co-precipitated with the minerals that formed in these treatments. Similar results were found in measurements of other heavy elements such as erbium, thulium, holmium and dysprosium (graphs attached in appendix).

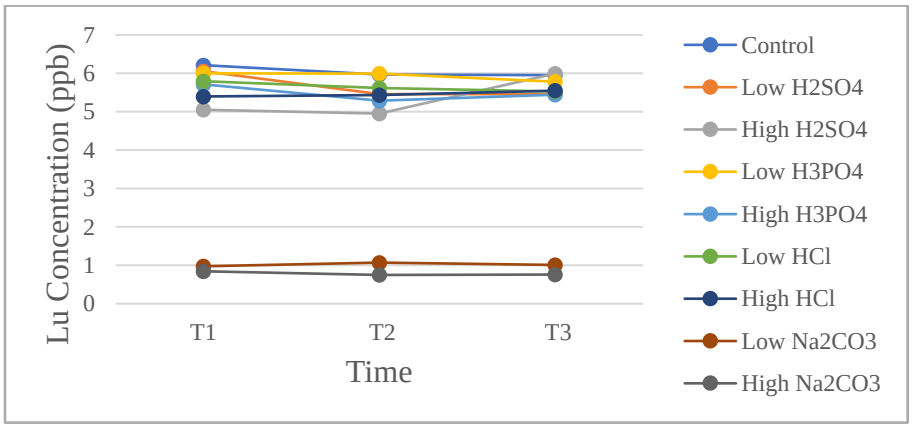

Figure 9: Comparison of lutetium concentrations over time between the different samples

Precipitate Chemistry

XRD results

XRD analysis allowed the identification of the mineral precipitates that formed in each bench experiment. The analysis of the control sample precipitates allowed for observations of the baseline conditions of the flowback fluid. Moreover, when compared to this control, it can be

seen how the different treatments resulted in the precipitation of different minerals. As shown in **Figure 10**, the XRD scan of the control sample has diffraction intensities that match patterns in the PDF 4+ database for akaganeite ($Fe^{3+}O(OH,Cl)$) and quartz (SiO_2). The quartz is likely a result of residual sand that is used in the hydraulic fracturing process. These data are consistent with analysis using ICP-OES in that the iron concentrations shown in **Figure 6** are lower for the control than most of the other treatments, indicating it is not in solution, and rather is precipitating in the form of akaganeite. This analysis is also consistent with SEM results.

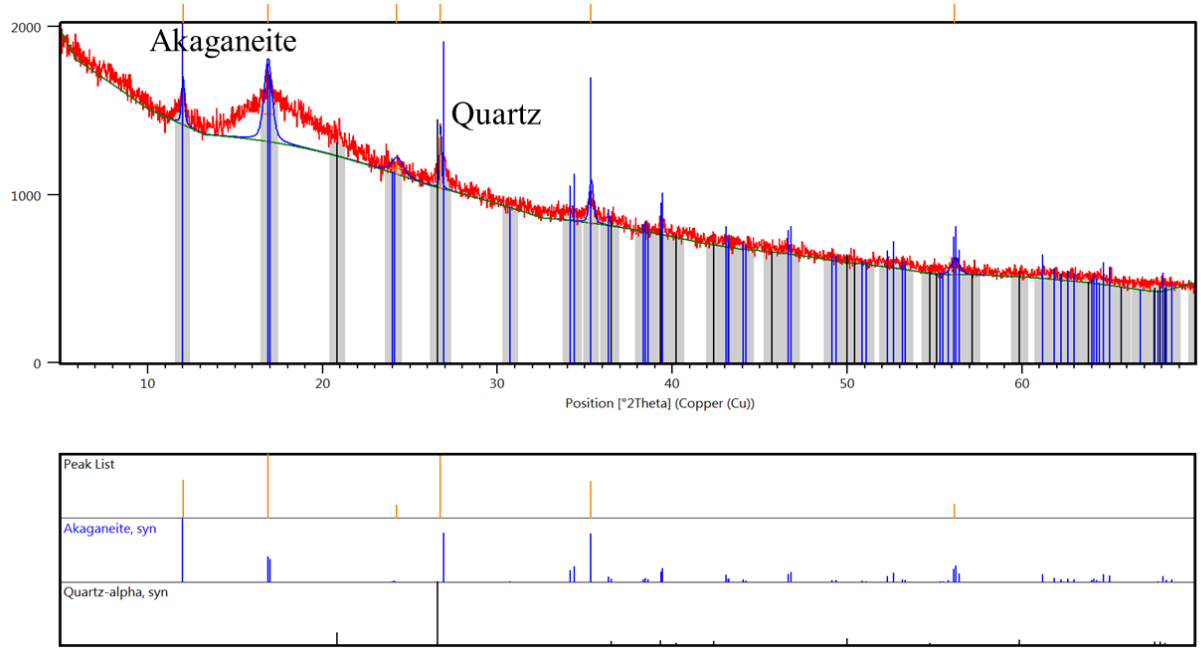

Figure 10: XRD analysis of the control sample

XRD measurements made on the low H_2SO_4 treatment indicate that the mineral constituents of the precipitate of this treatment are barite ($BaSO_4$) and quartz (SiO_2). This can be seen through the matched diffraction intensities that match patterns in the PDF 4+ database for these minerals (**Figure 11)**. Compared to the control precipitate, there is no longer an abundance of akaganeite due to the acidity of the sample causing the iron to dissolve, resulting in the high levels of iron seen in the corresponding solution of this sample, seen in the ICP-OES analysis depicted in **Figure 6**. ICP-OES analysis also indicates a decrease in barium concentration for the fluid of this sample, indicating it came out of solution as the barite seen in XRD analysis (**Figure 5**). The quartz is likely residual sand used in the hydraulic fracturing process. SEM analysis of this sample also shows the precipitation of barite (**Figure 14**).

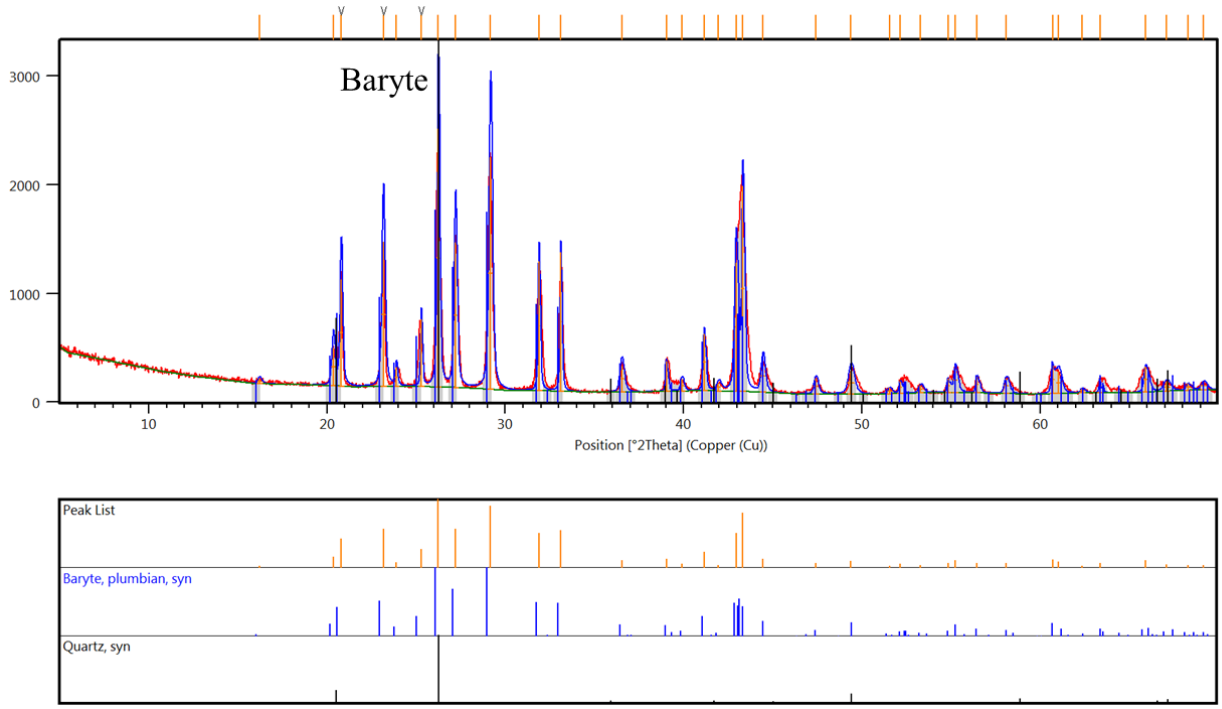

Figure 11: XRD analysis of the sample with the low H_2SO_4 treatment

Measurements made on the high H_2SO_4 treatment indicate that the precipitates that formed in the batch reactor are celestite ($SrSO_4$) and gypsum ($CaSO_4 \cdot 2H_2O$). The quartz (SiO_2) is likely residual sand from the hydraulic fracturing process. This is shown in **Figure 12**, which indicates the XRD scan has diffraction intensities that match patterns in the PDF 4+ database for these minerals. The akaganeite is not present in this sample due to the high acidity causing the iron to dissolve and remain in solution, as seen in the ICP-OES analysis of iron (**Figure 6**). ICP-OES analysis also shows decreases in calcium and strontium concentrations in the fluid sample of this experiment, which is consistent with the precipitation of gypsum and celestite, respectively (**Figures 3 & 4**). SEM analysis also indicates that the precipitate of this sample is gypsum and celestite (**Figure 15**).

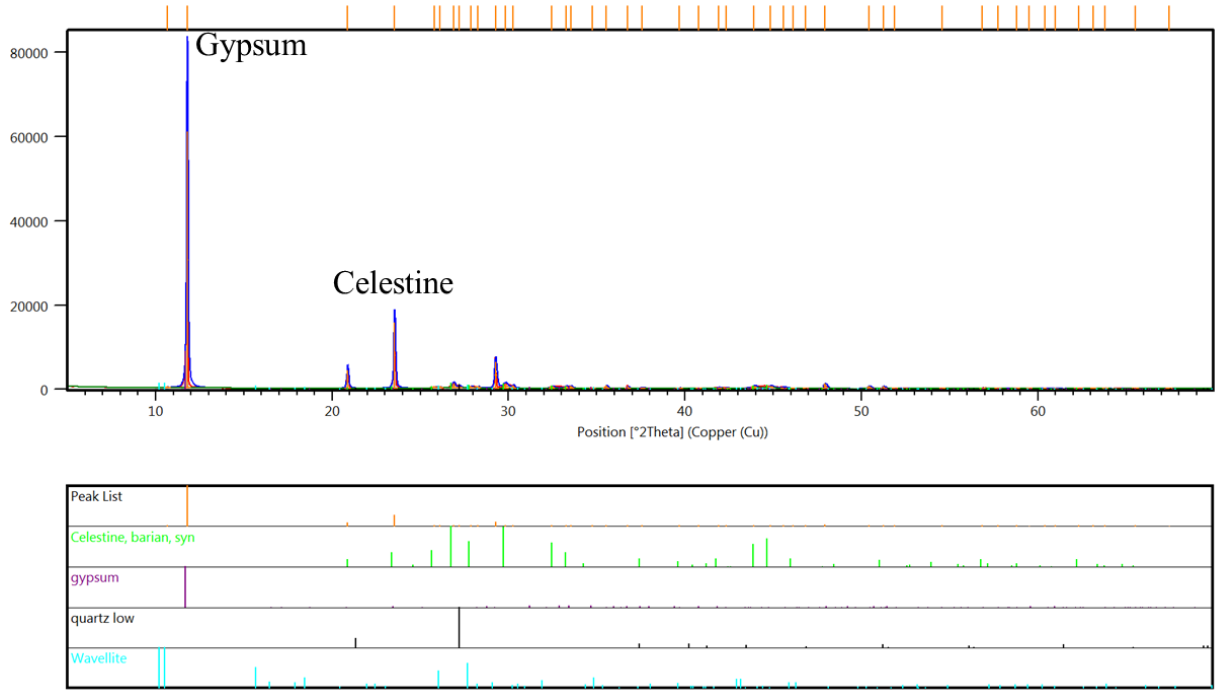

Figure 12: XRD analysis of the sample with the high H_2SO_4 treatment.

SEM Results

The SEM analysis helped identify the composition of the different minerals that precipitated out of each respective solution. When compared to one another, it can be seen how different treatments resulted in the precipitation of different minerals. Furthermore, even adding higher concentrations of the same treatment also resulted in the precipitation of different minerals or even the same minerals but with different morphologies.

Precipitates from the control sample were characterized to determine the baseline conditions and the effects of the different amendments on the chemistry and mineralogy of phases formed. A characteristic image of the precipitates from the control experiments is depicted in **Figure 13**. The groundmass is mostly akaganeite ($Fe^{3+}O(OH,Cl)$) and quartz (SiO_2), consistent with the results of the XRD analysis. The round, rosettes were determined to be celestite ($SrSO_4$), although few of them were found throughout the sample, as evidenced by their absence in the XRD analysis.

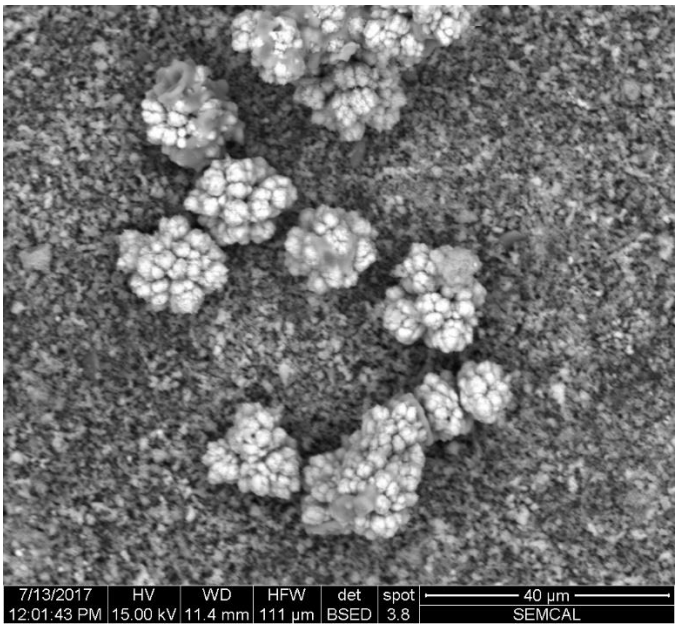

Figure 13: SEM image of the precipitate of the control sample.

In comparison to the control sample, the low H_2SO_4 treatment is much different. As seen in **Figure 14**, the akaganeite groundmass is no longer abundant and precipitate with a different morphology and chemistry formed. The round bulbous precipitates were determined to be barite ($BaSO_4$) with traces of strontium whereas the flat rectangular phases are almost pure, endmember barite ($BaSO_4$) based on spot analyses using an energy dispersive X-ray analyzer (EDX). These results are consistent with the ICP-OES data, which showed a decrease in barium concentration from 626.3 mg/L to 304.8mg/L (**Figure 5**). Even so, the initial barium concentration was much lower than in most of the other treatments, indicating that much of the barium probably precipitated out of solution rather rapidly. Strontium concentrations, as analyzed with ICP-OES seen in **Figure 4**, are lower than what is seen in the other treatments, indicating that is it being incorporated into this precipitate. These results are also consistent with XRD analysis.

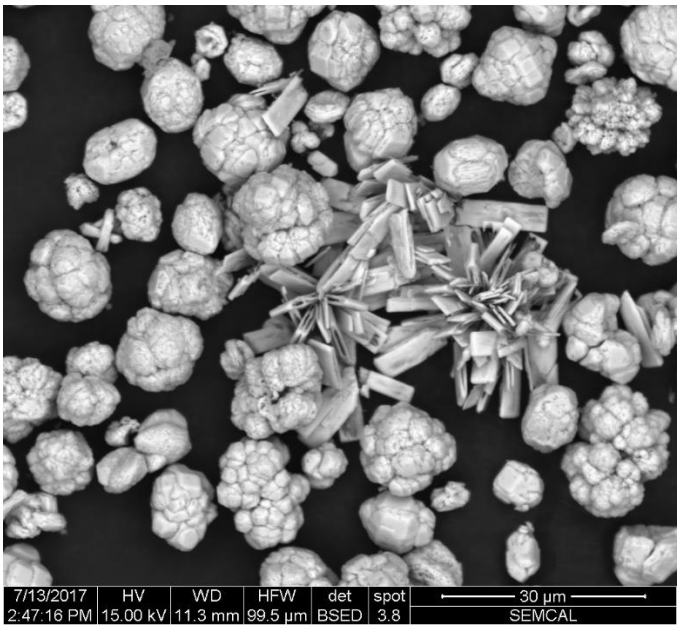

Figure 14: SEM image of the precipitate from the sample with the low H_2SO_4 treatment.

The precipitate that formed in the high H_2SO_4 treatment experiments is further distinguished from the control and even the low concentration of the same treatment. Some barite precipitates were observed, but the precipitate is mostly composed of large flat pieces determined to be gypsum ($CaSO_4 \cdot 2H_2O$) and the small flowerlike occurrences of celestite ($SrSO_4$), as seen in **Figure 15**. These results are consistent with both calcium and strontium ICP-OES data, in that concentrations of both calcium and strontium decreased over time for this sample, indicating that they came out as precipitate (**Figures 3&4**). Additionally, ICP-OES analysis indicates that the barium levels of the solution of this sample were much lower than the other samples, seen in **Figure 5**. This would indicate the precipitation of a barium mineral, however, there is not any pure barite minerals in this precipitate. This observation indicates that the barium must be incorporated elsewhere, likely into the celestite. These results are consistent with XRD analysis that indicated the precipitation of celestite and gypsum (**Figure 12**).

Figure 15: SEM image of the precipitate from the sample with the high H_2SO_4 treatment.

Much like the precipitate of the control, the precipitate of the low H_3PO_4 treatment is also composed of the flowerlike pieces of celestite ($SrSO_4$) and a groundmass of akaganeite ($Fe^{3+}O(OH,Cl)$) and quartz (SiO_2), as seen in **Figure 16**. There are no phosphate phase minerals despite the addition of phosphate. This could be due to the undersaturation of the constituents that would make up phosphate minerals. These results are consistent with the strontium ICP-OES data and the XRD analysis.

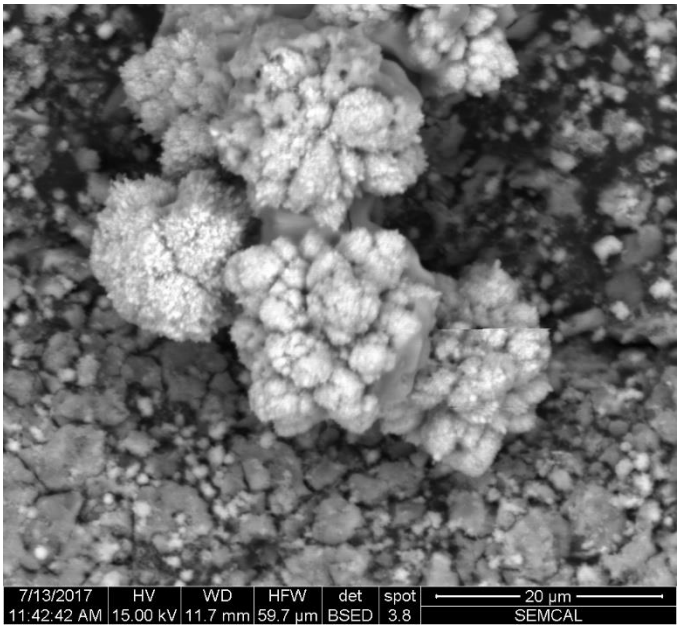

Figure 16: SEM image of the precipitate from the sample with the high H_3PO_4 treatment.

The high HCl precipitate shows very little mineral speciation, similar to the precipitate of the control and the high H_3PO_4 treatments. The main mineral constituents are barite, seen as the tiny bright flecks, and akaganeite and quartz (**Figure 17**). These results are consistent with ICP-OES analysis in that the solution chemistry does not change over time for most of the elements in this sample, indicating that they did not come out of solution. The iron concentration plateaus by the third time point, indicating it could be providing the iron for akaganeite (**Figure 6**) and the quartz is likely residual sand used in the hydraulic fracturing process.

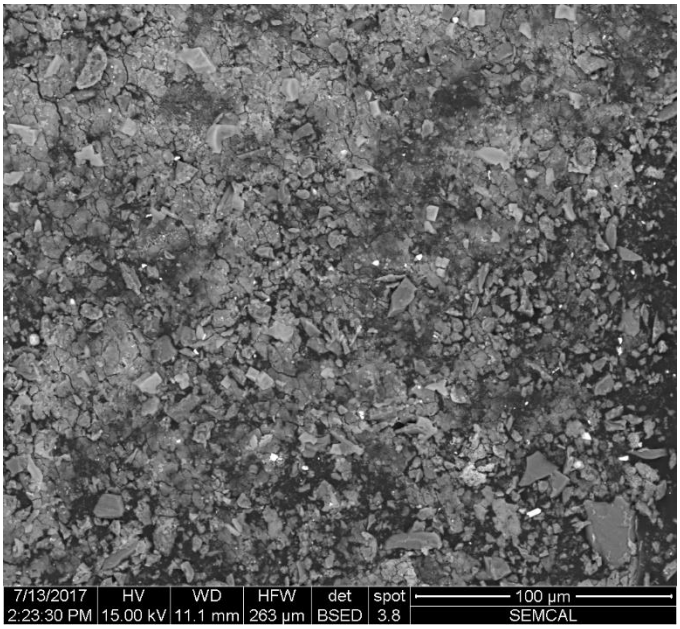

Figure 17: SEM image of the precipitate from the sample with the high HCl treatment.

The precipitate that formed in the high Na_2CO_3 treatment is mainly composed of calcite ($CaCO_3$) (**Figure 18**). These results are consistent with ICP-OES results which show lowered amounts of calcium over time, which indicate that it precipitated out. Based upon spot analysis using EDX, this precipitate has elevated levels of strontium, barium, and iron, indicating that these elements co-precipitated with the precipitation of calcite. This is consistent with ICP-OES analysis of these elements, as depicted in **Figures 4-6**.

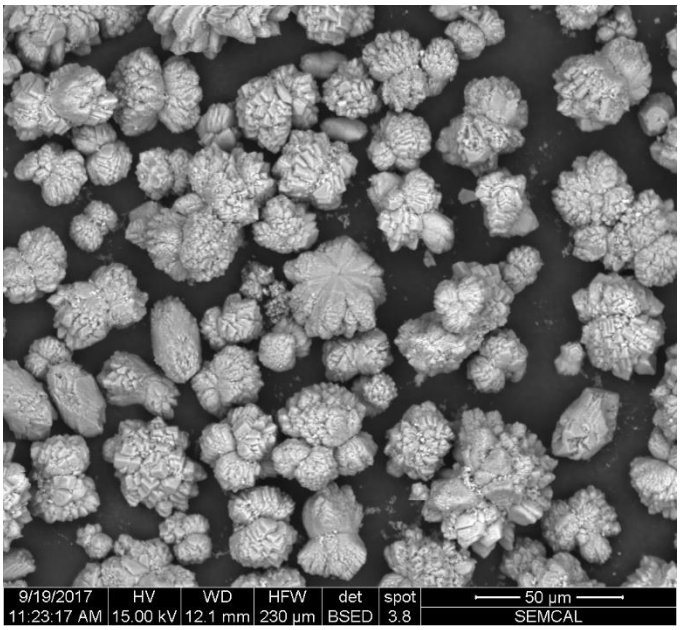

Figure 18: SEM image of the precipitate from the sample with the high Na_2CO_3 treatment.

DISCUSSION

The large volumes of flowback fluids generated from hydraulic fracturing can present environmental issues such as exposing the surrounding areas to naturally occurring radioactive materials or toxic elements that come out of these wells. However, if we can treat and reuse these fluids we can minimize these environmental impacts. In addition, these fluids may contain elevated concentrations of trace metals (such as the REE) that have been extracted from the formation that may represent an economic benefit.

XRD, SEM, and ICP-OES/MS analyses showed that the mixing of hydraulic fracturing flowback fluid (HFFF) and different acids and bases produces reductions of key elements that are originally present in the HFFF. Decreased levels of calcium, strontium, and barium, result from the low H_2SO_4, high H_2SO_4, and high Na_2CO_3 treatments (**Figures 3-5**). However, in the phosphate and chloride treatments, very little change is seen from these samples compared to the control, in both the solution chemistries and the SEM images of the precipitates. This suggests that the original HFFF chemistry and the type of additive determine the magnitude and type of element removal.

Results of the sulfate amendment treatments are consistent with other studies that used HFFF and synthetic acid mine drainage (AMD), a sulfate-rich fluid, to induce precipitation to selectively remove barium and radium from the fluids (Kondash et al., 2014). In their studies, Kondash et al. demonstrated that their mixing experiments removed 100% of the sulfate, nearly 100% of the radium and barium, and up to 70% of the strontium through the precipitation of different minerals. The minerals that formed in their experiment were mostly barite, celestite, calcite, gibbsite, and gypsum, occurring in various concentrations depending on the ratio of HFFF to AMD (Kondash et al., 2014). These results are largely consistent with those from our own experiment as seen in the similarities between the types of elements and minerals that precipitated.

The lowered concentrations of barium seen in **Figure 5**, specifically in the low H_2SO_4 and high H_2SO_4 treatments, can largely be attributed to the precipitation of barite and barite-celestite phases. The morphology of the crystals is a good indication of the processes that occurred and the saturation state of the fluid (Dunn et al., 1999). It is likely the precipitation began with nucleation at random points within the experimentation bottles and then more layers grew upon them, forming rhombic tabular crystals. Concretion of these tabular barite crystals, caused by continuous nucleation and growth of smaller crystals on larger ones, take the form of rosettes (Dunn et al., 1999), like those seen in **Figure 14**, of the low H_2SO_4 treatment. The shapes of barite crystal can be a good indication of the conditions in which they grew. The degree of supersaturation is a factor that largely controls to the morphology of barite crystals. The shapes seen in the current work, namely, the tabular and the rosette balls that form from the tabular pieces (**Figure 14**), indicate that the crystal growth was controlled by the diffusional transport of solute from the HFFF to the surface of growing crystals in the bottle, formed from the aqueous solution with high degrees of supersaturation (Dunn et al., 1999). The precipitates formed in the Dunn et al. experiment had a similar habit to those seen in our own experiment, the barite clusters made up of tabular crystals, indicating similar degrees of saturation in the respective fluids of each experiment of about 4.0. Furthermore, this idea is consistent with PHREEQC modeling of the fluids of our experiment that calculated speciation and saturation indexes (SI) of different mineral phases (**Table 2**). This modeling indicates that the SI for the low and high H_2SO_4 treatments are 4.04 and 5.11, respectively.

The barite formed in this experiment could potentially incorporate radium, a NORM that could be present in the flowback fluid. He et al. (2016) found that the barite formed in their experiments when flowback water from hydraulic fracturing was mixed with abandoned mine drainage, incorporated 99% of the radium present in the flowback water. This is due to the similar ionic radii of radium and barium, their electronic configuration, and the identical crystallographic structure of $RaSO_4$ and $BaSO_4$, resulting in co-precipitation of radium with both barite and celestite minerals (Kondash et al., 2014). This co-precipitation could help control the proper disposal of NORM such as radium that could be brought to the surface through the hydraulic fracturing process.

The lowered levels of strontium seen in **Figure 4**, specifically in the high H_2SO_4 treatment, is likely due to the precipitation of celestite. SEM images of the celestite produced in this treatment can be seen in **Figure 15**. It is possible that these lowered levels are only observed in the high H_2SO_4 sample and not the low as well, such as what was observed with barium concentrations, because sulfate is a better removal agent of barium than strontium because barite ($BaSO_4$) solubility is approximately three orders of magnitude lower than that of celestite ($SrSO_4$) (He et al., 2014).

This difference in solubility suggests that higher concentrations of sulfuric acid would need to be added in order to achieve significant strontium removal (He et al., 2014). In their experiment, He et al. combined synthetic HFFF with different doses of $NaSO_4$. In doing so, in all experiments and dosages, barite precipitated much faster and to a higher degree than celestite (He et al., 2004). However, when sulfate concentrations were increased, the strontium removal efficiency also increased, but never to the same degree as the barium removal (He et al., 2014). These results can help explain why a much lower strontium concentration is seen in the ICP-OES analysis of the high H_2SO_4 treatment compared to the low in our experiment (**Figure 4**) and why we see more celestite precipitate from that same treatment in the SEM analysis (**Figure 15**).

The precipitation of gypsum seen in the high H_2SO_4 treatment (**Figure 15)** is likely a result of the high sulfate and calcium concentration in the solution. A study on the solubility of celestite and barite in electrolyte solutions and natural waters found that in their system of $SrSO_4$-$CaCl_2$-H_2O resulted in celestite solubility increased with the $CaCl_2$ concentration up to a point where $SrSO_4$ becomes more soluble than gypsum, which is then the phase that controls the sulfate content of the solution (Monnin & Galinier, 1988). In other words, the dissolution of celestite in calcium rich solutions results in the formation of $CaSO_4{\cdot}2H_2O$ as a secondary phase (Monnin & Galinier, 1988). The experiments of Kondash et al. (2014) found that gypsum was a precipitate that formed only when the ratio of AMD to HFFF was highest, of 75% AMD to 25% HFFF. Because their AMD solution consisted largely of sulfate, their results are consistent with our own experiment as gypsum was only a precipitate in the high H_2SO_4 treatment.

The high and low additions of both H_3PO_4 and HCl treatments results differ greatly from the others in that very little precipitation occurred. Compared to the sulfate treatments, they are all of similar pH, with only the anion as different, so these largely different results were not expected. However, using saturation index modeling of these fluids using PHREEQC, it indicates that almost all mineral phases are largely undersaturated in these solutions, causing them to remain in solution. For example, one might expect to precipitate phosphate minerals such as strengite ($FePO_4{\cdot}2H_2O$) or vivianite ($Fe_3(PO_4)_2{\cdot}8(H_2O)$) upon the addition of phosphoric acid. However, PHREEQC modeling suggests that these minerals have SI of -11.82 and -30.41, respectively, in

the high H_3PO_4 solutions, indicating that they are very highly undersaturated, explaining the lack of precipitation observed (**Table 2**).

Part of the purpose of this experiment was to explore how the precipitation of iron minerals, specifically jarosite group minerals, could influence the sequestration of major and trace elements from solution. However, seen in **Figure 6**, the iron concentrations in the solutions increased over time, indicating that the iron that already existed as suspended solid in the HFFF, dissolved rather than creating new minerals. In a study on the influence of pH on the mineral speciation of iron when combined with simulated acid mine drainage, it was found that minor changes in pH can have important impacts within acid SO_4 systems (Bingham et al., 1996). This study found that jarosite was produced when combined with sulfuric acid containing solutions at a pH of 2.3 and below. When compared to the results of our own study, the pH of the system, specifically in both H_2SO_4 treatments, was within that of the Bingham study, measured at 1.03 and 0.14, respectively (**Table 1**), however, there is no jarosite precipitation. This can be explained by looking at PHREEQC modeling on these solutions, which indicates a SI of -43.01 and -46.12. These solutions, as well as all the other solutions, are severely undersaturated with respect to jarosite, resulting in the absence of its precipitation (**Table 2**).

	Saturation Index (SI)								
Mineral	Control	Low H_2SO_4	High H_2SO_4	Low H_3PO_4	High H_3PO_4	Low HCl	High HCl	Low Na_2CO_3	High Na_2CO_3
Anhydrite	-2.38	0.00	0.99	-2.38	-2.36	-2.38	-2.38	-2.38	-2.39
Barite	1.65	4.04	5.11	1.67	1.94	1.65	1.65	1.66	1.70
Calcite	-	-	-	-	-	-	-	0.94	2.31
Celestite	-1.07	1.31	2.32	-1.09	-1.24	-1.07	-1.07	-1.06	-1.05
Ferrihydrite	-13.24	-17.29	-19.94	-16.40	-18.05	-15.83	-19.19	-1.80	-0.95
Gypsum	-2.26	0.12	1.11	-2.26	-2.24	-2.26	-2.27	-2.26	-2.27
K-Jarosite	-39.69	-43.01	-46.12	-45.91	-48.11	-44.88	-51.82	-16.95	-15.24
Quartz	0.97	0.97	0.98	0.97	0.94	0.97	0.99	0.97	0.96
Strengite	-10.88	-13.57	-15.27	-12.22	-11.82	-12.62	-14.97	-3.61	-3.23
Strontianite	-	-	-	-	-	-	-	0.79	2.18
Vivianite	-28.71	-34.11	-37.47	-31.37	-30.41	-32.19	-36.98	-14.39	-13.90
Witherite	-	-	-	-	-	-	-	-0.55	0.87

Table 2: PHREEQC speciation and saturation-index modeling calculations

The low pH values measured in each solution (**Table 1**) can help explain why there is not much change in the REE or trace metal concentrations of the solutions. A study based in Yellowstone National Park, Wyoming aimed at exploring the REE geochemistry of the acid-sulphate and acid-sulphate-chloride geothermal systems on the area found that springs with the lowest pH tended to have the highest sum of REE contents (Lewis et al., 1997). They concluded that REE are readily released into solution during dissolution of minerals and volcanic rocks of the surrounding area by circulating low pH fluids and that pH is a major factor affecting the ability

of a fluid to mobilize and transport REE (Lewis et al., 1997). The pH values of the water samples Lewis et al. measured ranged from 2 to 4, with the pH 2 samples always having the highest concentration of REE. With the pH values measured in this set of experiments having been in that range for the acid additions, if not lower, it makes sense that many of the REE and trace metal measurements did not change much through time (**Figures 7-9**).

A study on the metal sorption on mineral surfaces concluded that most metal sorption on hydrous ferric oxide increases with increasing pH (Smith, 1999). This could explain why there are trends of trace metals being removed from solution primarily by the carbonate treatments (**Figures 7-9**), as the pH in these treatments are 6.26 and 6.64 for the low and high treatments, respectively. This more neutral pH allows the metals to co-precipitate more readily with the calcite precipitates of these treatments.

CONCLUSIONS

Reaction of hydraulic fracturing fluid with different acids and bases in different concentrations allowed for the precipitation of different minerals with variable elemental compositions. Low concentrations of H_2SO_4 added to the flowback fluid resulted in the precipitation of mainly barite, whereas high concentrations of H_2SO_4 resulted in the precipitation of celestite and gypsum. The difference in these two precipitates, despite having the same kind of additive, is likely due to the saturation state of the fluid and the solubility of the respective minerals. However, both barite and celestite are advantageous precipitates because they could help sequester any naturally occurring radioactive materials that may be present in these fluids.

The low and high concentrations of the HCl and H_3PO_4 treatments largely did not result in the precipitation of any mineral phases, therefore, resulting in the lack of co-precipitation of any additional trace metals. These results can be explained through the undersaturation of any potential minerals given the constituents of the fluids. Undersaturation also resulted in the lack of precipitation of jarosite group minerals, despite being in the right pH range to do so.

Na_2CO_3 treatments of HFFF resulted in the most successful removal of trace elements. The solution chemistries of these samples indicate that precipitates formed were able to co-precipitate many trace metals, including lanthanum and lutetium. These results are most likely a function of the solution pH due to the fact that metals more readily sorb with increasing pH, as it approaches neutral, and these solutions have nearly neutral pH values.

With enormous amounts of HFFF being produced around the country, it is beneficial to all to improve the quality of these fluids. The results of this study can be used to develop methods for the hydraulic fracturing process to seek its improvement. This study demonstrates how flowback fluids can be treated for possible reuse through the removal of toxic or radioactive elements. It also showed that certain treatments could create flowback fluids as a potential source for trace elements in concentrations that could render them economically viable.

RECOMMENDATIONS FOR FUTURE WORK

In future work on this project, one could make several samples of each amendment in order to better estimate the precision of the mineral precipitation induced by each treatment. In addition, one could use the observations and conclusions made here to further explore the behavior and sorption potential of akaganeite. Also, using similar methods that were used in this study, further research could quantitatively measure how efficient these methods were at removing NORM. In further exploration of the subject matter of this project, one could use the observations and conclusions made here to determine how certain additives to HFFF can precipitate different elements and minerals of interest. Further research could include additives of acids with the goal to create a pH that falls into the jarosite stability range and with proper saturation to achieve better co-precipitation and sorption of trace metals and REE. Further research could incorporate additives such as sulfate rich acid mine waste to induce precipitation of sulfate minerals or jarosite group minerals. Also, new research could take a slightly different approach and focus on additives that could induce oxidation or biological activity to sequester metals from flowback fluids by biologically mediated sorption-precipitation reactions.

REFERENCES CITED

Bigham, J.M., Schwertmann, U., and Pfab, G., 1996, "Influence of pH on mineral speciation in a bioreactor simulating acid mine drainage." *Applied Geochemistry*, vol. 11, no. 6, pp. 845–849., doi:10.1016/s0883-2927(96)00052-2

Chen, H., and Carter, K.E., 2016, "Water usage for natural gas production through hydraulic fracturing in the United States from 2008 to 2014." *Journal of Environmental Management*, vol. 170, pp. 152–159., doi:10.1016/j.jenvman.2016.01.023.

Dunn, K., Daniel, E., Shuler, P.J., Chen, H.J., Tang, Y., and Yen, T.F., 1999, "Mechanisms of Surface Precipitation and Dissolution of Barite: A Morphology Approach." *Journal of Colloid and Interface Science*, vol. 214, no. 2, pp. 427–437., doi:10.1006/jcis.1999.6224

He, C., Li, M., Liu, W., Barbot, E., and Vidic, R.D., 2014, "Kinetics and Equilibrium of Barium and Strontium Sulfate Formation in Marcellus Shale Flowback Water." *Journal of Environmental Engineering*, vol. 140, no. 5, doi:10.1061/(asce)ee.1943-7870.0000807.

He, C., Zhang, T., and Vidic, R.D., 2016, "Co-Treatment of abandoned mine drainage and Marcellus Shale flowback water for use in hydraulic fracturing." *Water Research*, vol. 104, pp. 425–431., doi:10.1016/j.watres.2016.08.030.

King, H., n.d. "Utica Shale - The Natural Gas Giant Below the Marcellus: geology.com/articles/utica-shale/. (accessed November 14, 2017)

Kondash, A.J., Warner, N.R., Lahav, O., and Vengosh, A., 2014, "Radium and Barium Removal through Blending Hydraulic Fracturing Fluids with Acid Mine Drainage." *Environmental Science & Technology*, vol. 48, no. 2, pp. 1334–1342., doi:10.1021/es403852h.

Lewis, A.J., Palmer, M.R., Sturchio, N.C., and Kemp, A.J., 1997, "The rare earth element geochemistry of acid-Sulphate and acid-Sulphate-Chloride geothermal systems from Yellowstone National Park, Wyoming, USA." *Geochimica et Cosmochimica Acta*, vol. 61, no. 4, pp. 695–706., doi:10.1016/s0016-7037(96)00384-5.

Monnin, C., and Galinier, C.. 1988, "The solubility of celestite and barite in electrolyte solutions and natural waters at 25°C: A thermodynamic study." *Chemical Geology*, vol. 71, no. 4, pp. 283–296., doi:10.1016/0009-2541(88)90055-1

Nelson, A.W., Eitrheim, E.S., Knight, A.W., May, D., Mehrhoff, M.A., Shannon, R., Litman, R., Burnett, W.C., Zorbes, T.Z., and Schultz, M.K., 2015, "Understanding the Radioactive Ingrowth and Decay of Naturally Occurring Radioactive Materials in the Environment: An Analysis of Produced Fluids from the Marcellus Shale", *Environmental Health Perspectives*, vol. 123, pp. 689-696

Riley R.A., 2015, Regional drilling activity and production, in Patchen, DG and Carter, KM, eds., *A geologic play book for Utica Shale Appalachian basin exploration, Final report of the Utica Shale Appalachian basin exploration consortium,* p. 11-19, Available from: http://www.wvgs.wvnet.edu/utica.

Smith, K.S., 1999, "Metal Sorption on Mineral Surfaces: An Overview with Examples Relating to Mineral Deposits." *Review in Economic Geology*, 6A , pp. 161–182

APPENDIX

Element	Concentration (ppm)
Na	53804.685
Mg	2199.208
K	1303.284
Ca	18724.959
Si	17.889
Sr	4607.724
Ba	1664.4408
Li	85.827
Fe	172.5518
Mn	8.352555
TDS (mg/L)	206014
TDS (g/L)	201.01

Chemistry of HFFF right after collection

Component	Percent Concentration
Aluminum	0.01
Arsenic	0.01
Barium Nitrate	0.01 (as Ba)
Barium Carbonate	0.01 (as Ba)
Beryllium Acetate	0.01 (As Be)
Bismuth	0.01
Boric Acid	0.01 (as B)
Calcium Carbonate	0.01 (as Ca)
Cadmium	0.01
Cerium Oxide	0.01 (as Ce)
Cesium Carbonate	0.01 (as Cs)
Chromium	0.01
Cobalt	0.01
Copper	0.01
Dysprosium Oxide	0.01 (as Dy)
Erbium Oxide	0.01 (as Er)
Europium Oxide	0.01 (as Eu)
Gadolinium Oxide	0.01 (as Gd)
Gallium	0.01
Holmium Oxide	0.01 (as Ho)
Indium	0.01
Iron	0.01
Lanthanum Oxide	0.01 (as La)
Lead	0.01
Lithium Carbonate	0.01 (as Li)
Lutetium Oxide	0.01 (as Lu)
Magnesium	0.01
Manganese Acetate Tetrahydrate	0.01 (as Mn)
Neodymium Oxide	0.01 (as Nd)
Nickel	0.01
Ammonium Dihydrogen Phosphate	0.01 (as P)
Potassium Nitrate	0.01 (as K)
Praseodymium Oxide	0.01 (as Pr)
Rhenium	0.01
Rubidium Nitrate	0.01 (as Rb)
Samarium Oxide	0.01 (as Sm)
Scandium Oxide	0.01 (as Sc)
Selenium	0.01
Sodium Carbonate	0.01 (as Na)
Strontium Nitrate	0.01 (as Sr)
Terbium Oxide	0.01 (as Tb)
Thallium	0.01
Thorium Oxide	0.01 (as Th)
Thulium Oxide	0.01 (as Tm)
Uranium Oxide	0.01 (as U)
Ammonium Metavanadate	0.01 (as V)
Ytterbium Oxide	0.01 (as Yb)
Yttrium Oxide	0.01 (as Y)
Zinc	0.01
Nitric Acid	4
Water, deionized	Balance

Composition of trace metal spike

ICP-MS Analysis

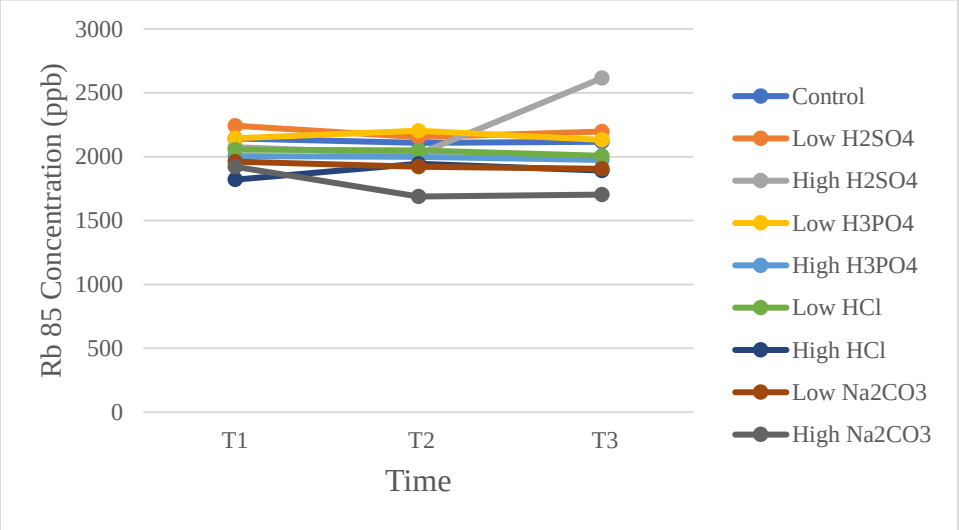

Comparison of rubidium concentrations over time between the different samples

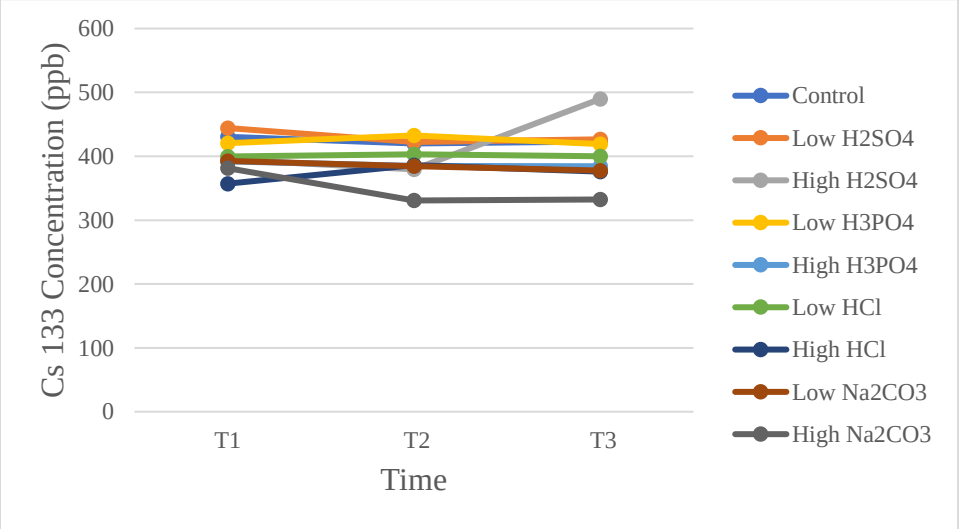

Comparison of cesium concentrations over time between the different samples

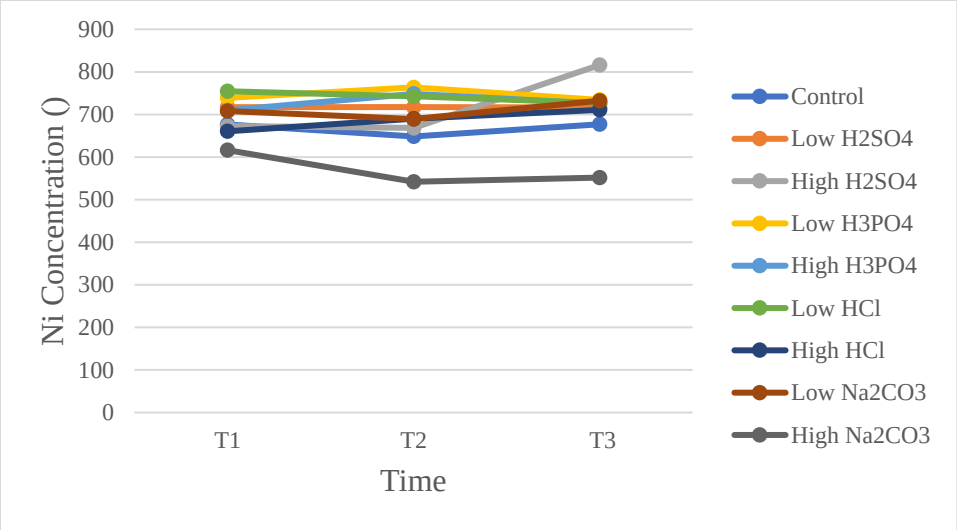

Comparison of nickel concentrations over time between the different samples

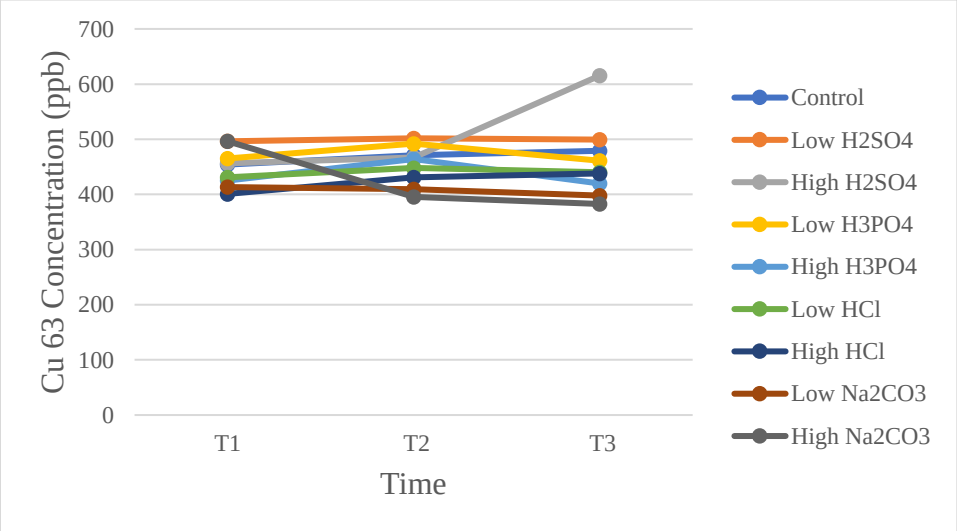

Comparison of copper concentrations over time between the different samples

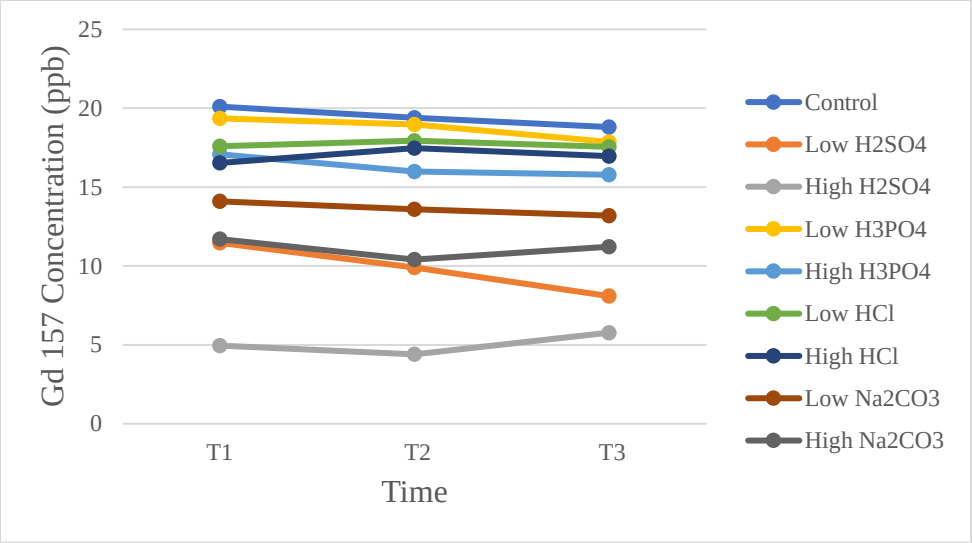

Comparison of gadolinium concentrations over time between the different samples

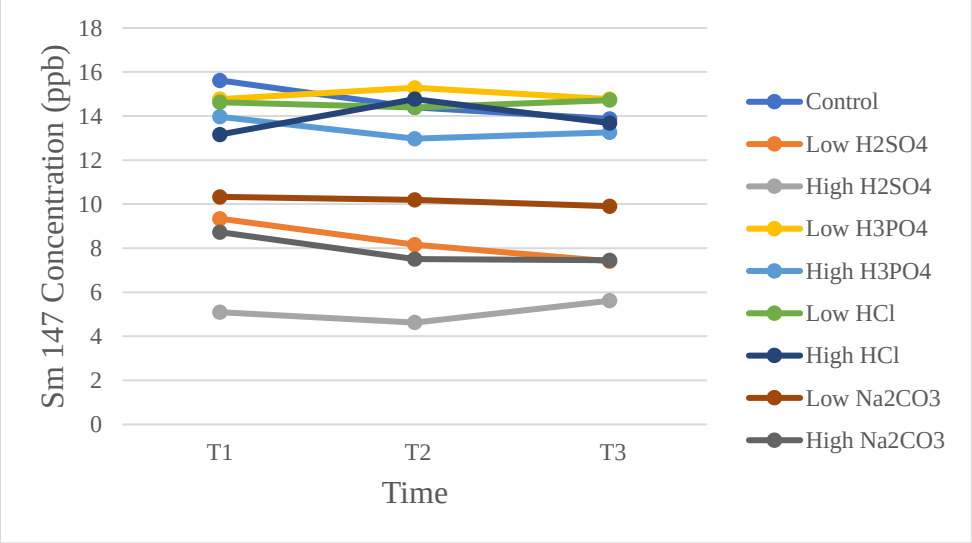

Comparison of samarium concentrations over time between the different samples

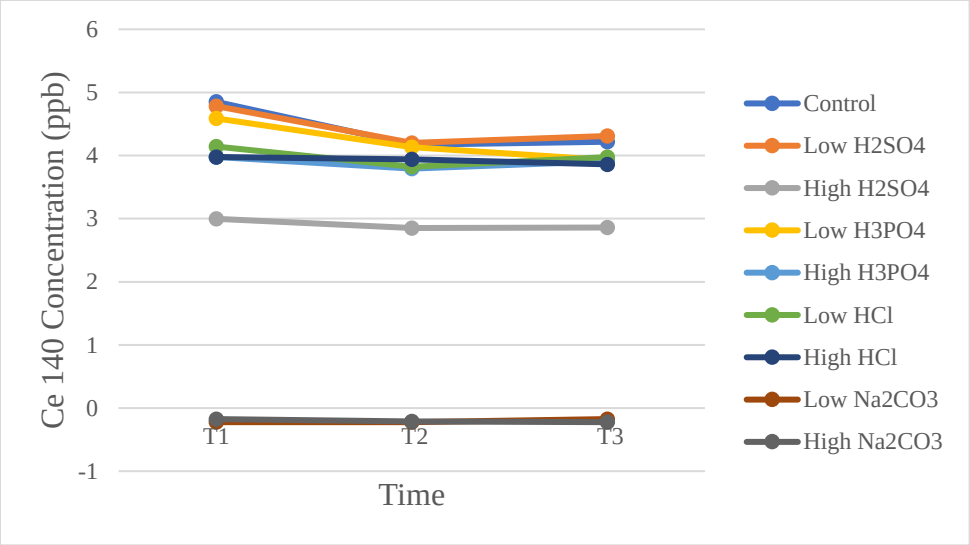

Comparison of cerium concentrations over time between the different samples

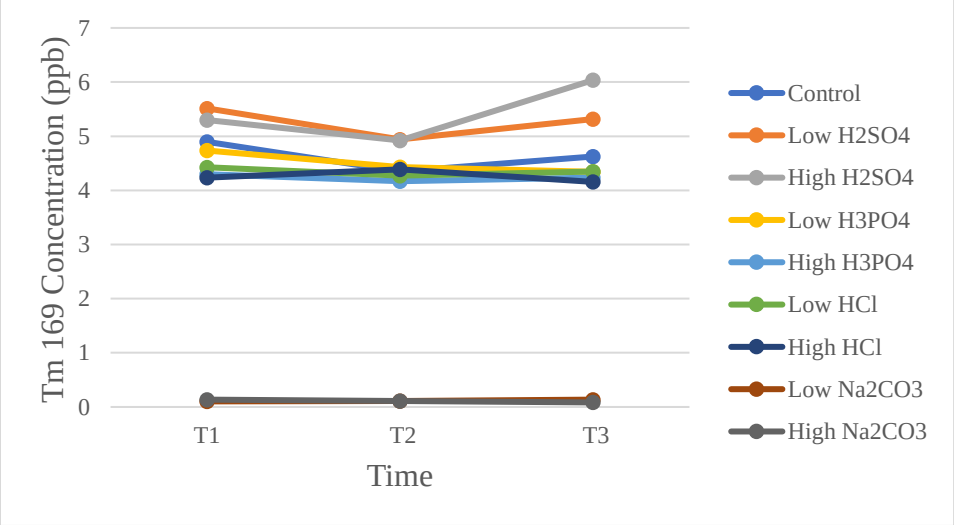

Comparison of thulium concentrations over time between the different samples

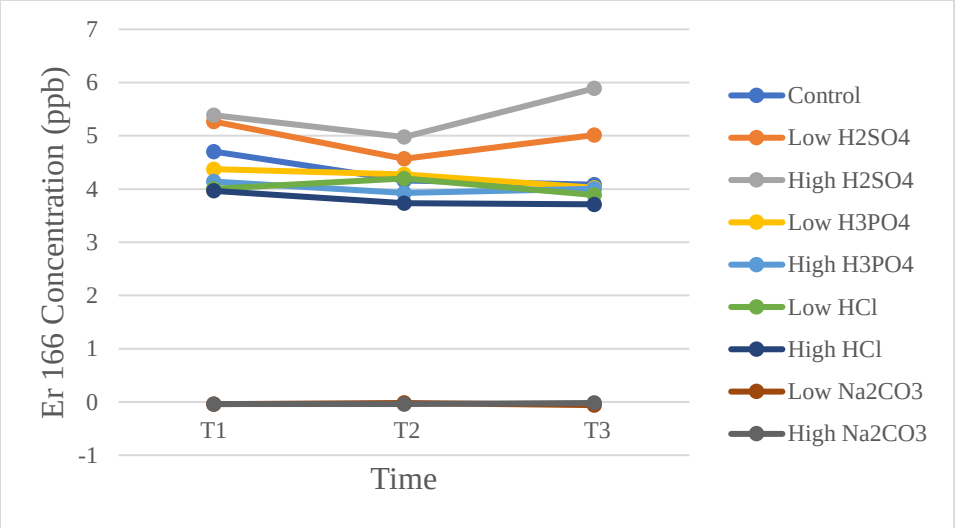

Comparison of erbium concentrations over time between the different samples

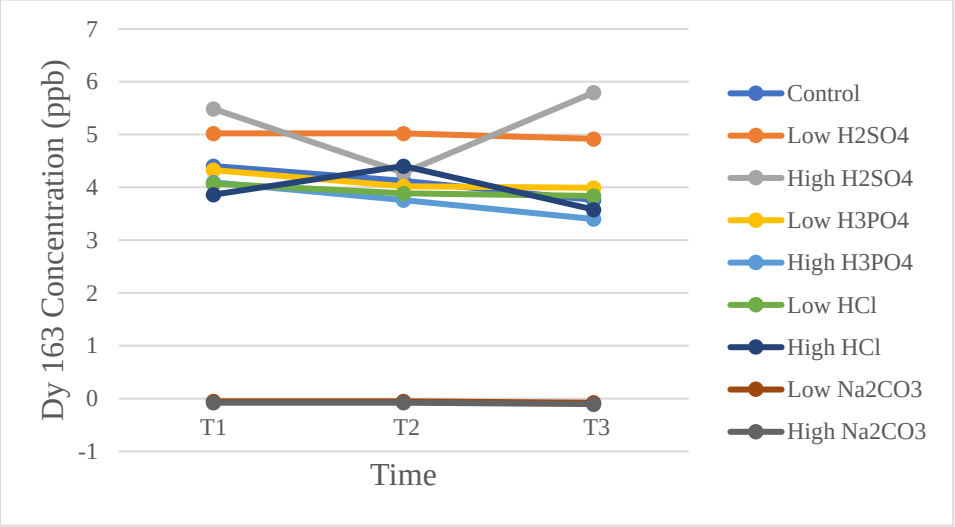

Comparison of dysprosium concentrations over time between the different samples

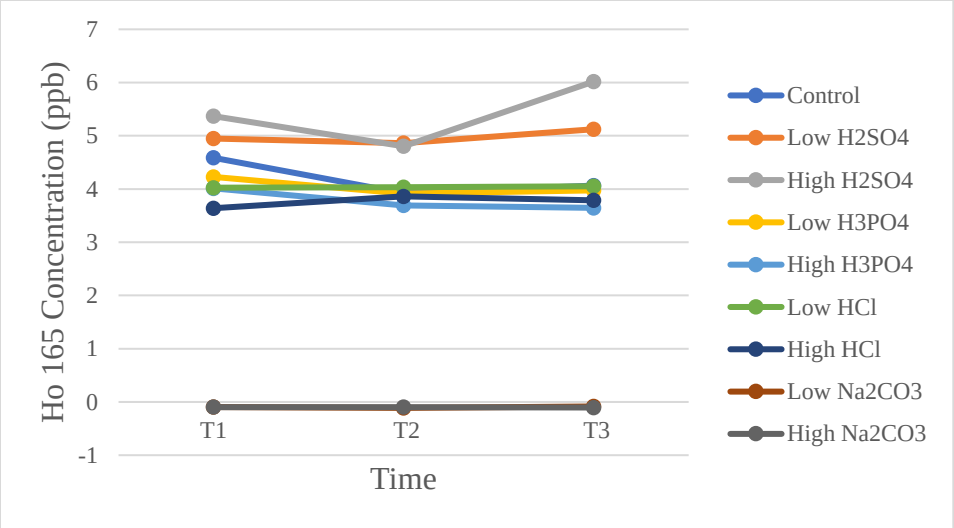

Comparison of holmium concentrations over time between the different samples

PHREEQC Saturation Indexes

Mineral	Control	Low H_2SO_4	High H_2SO_4	Low H_3PO_4	High H_3PO_4	Low HCl	High HCl	Low Na_2CO_3	High Na_2CO_3
Anhydrite	-2.38	0.00	0.99	-2.38	-2.36	-2.38	-2.38	-2.38	-2.39
Aragonite	-	-	-	-	-	-	-	0.76	2.13
Barite	1.65	4.04	5.11	1.67	1.94	1.65	1.65	1.66	1.70
CaHPO4	-1.78	-3.13	-4.04	-2.11	-1.76	-2.64	-3.75	1.77	1.91
CaHPO4:2H2O	-2.19	-3.54	-4.46	-2.52	-2.17	-3.05	-4.16	1.37	1.50
Calcite	-	-	-	-	-	-	-	0.94	2.31
Celestite	-1.07	1.31	2.32	-1.09	-1.24	-1.07	-1.07	-1.06	-1.05
Chalcedony	0.52	0.52	0.53	0.52	0.49	0.52	0.54	0.52	0.51
Dolomite	-	-	-	-	-	-	-	0.76	3.54
Ferrihydrite	-13.24	-17.29	-19.94	-16.40	-18.05	-15.83	-19.19	-1.80	-0.95
Fluorite	-2.92	-2.97	-3.27	-2.88	-2.58	-2.94	-3.19	-2.90	-2.77
Goethite	-10.47	-14.52	-17.18	-13.64	-15.28	-13.06	-16.43	0.96	1.82
Gypsum	-2.26	0.12	1.11	-2.26	-2.24	-2.26	-2.27	-2.26	-2.27
Hydroxylapatite	-	-	-	-	-	-	-	19.70	21.30
K-Jarosite	-39.69	-43.01	-46.12	-45.91	-48.11	-44.88	-51.82	-16.95	-15.24
Quartz	0.97	0.97	0.98	0.97	0.94	0.97	0.99	0.97	0.96
Siderite	-	-	-	-	-	-	-	-6.92	-5.67
SiO2(am-gel)	-0.32	-0.32	-0.31	-0.32	-0.35	-0.32	-0.30	-0.32	-0.33
SrHPO4	-2.71	-4.06	-4.96	-3.07	-2.88	-3.57	-4.68	0.86	1.00
Strengite	-10.88	-13.57	-15.27	-12.22	-11.82	-12.62	-14.97	-3.61	-3.23
Strontianite	-	-	-	-	-	-	-	0.79	2.18
Thenardite	-6.77	-4.39	-3.30	-6.74	-6.36	-6.78	-6.82	-6.75	-6.63
Vivianite	-28.71	-34.11	-37.47	-31.37	-30.41	-32.19	-36.98	-14.39	-13.90
Witherite	-	-	-	-	-	-	-	-0.55	0.87